ORGANIC CHEMISTRY FRONTIERS

RESEARCH ARTICLE

View Article Online
View Journal | View Issue

Cite this: *Org. Chem. Front.*, 2024, **11**, 6627

Strongly fluorescent indolizine-based coumarin analogs†

Jaqueline S. A. Badaro, [a] Antoni Wrzosek, [b] Olaf Morawski, [c] Adam Szewczyk, *[b] Irena Deperasińska *[c] and Daniel T. Gryko *[a]

It is now possible to prepare 2-oxo-2*H*-pyrano[2,3-*b*]indolizine-3-carboxylates with an ordered arrangement of various substituents directly from pyridinium salts and diethyl 2-(ethoxymethylene)malonate, allowing for refined control of their photophysical properties. Facile entry into some previously unknown derivatives is disclosed to demonstrate the potential of this method. The use of substituted picolinium salts, as well as further functionalization of the pyrrole ring, permitted easy introduction of new moieties upon the dye, which enabled fine-tuning of the photophysical properties. The obtained dyes possess absorption and emission spectrum in the blue–green region and fluorescence quantum yields reaching 92%. The parent 2-oxo-pyrano[2,3-*b*]indolizine-3-carboxylate turned out to be an electron-deficient system with a low-lying LUMO, an electronic transition energy of 2.7 eV and possessing a large oscillator strength. Almost complete overlap of the HOMO and LUMO in the 2-oxo-pyrano[2,3-*b*]indolizine core is responsible for the large fluorescence quantum yields for almost all prepared derivatives. The reason for maintaining the large emission intensity in polar solvents is that the increase in the dipole moment is accompanied with a significant change in its orientation in space. Fluorescence imaging studies have proven that 2-oxo-pyrano[2,3-*b*]indolizines penetrate the membrane of living cells. A positively charged analog was synthesized and used to stain intracellular organelles in the H9c2 cell line. This compound did not penetrate the cell membrane, however after permeabilization, it specifically stained the nucleus.

Received 3rd July 2024,
Accepted 10th September 2024

DOI: 10.1039/d4qo01216j

rsc.li/frontiers-organic

Introduction

Pyrano[2,3-*b*]indolizin-2-ones are a unique class of heterocycles that, contrary to their analogues pyrano[3,2-*b*]indol-2-ones[1–12] and pyrano[2,3-*b*]indol-2-ones,[13–22] have been greatly ignored after they were synthesized by Kakehi *et al.* in the 80s[23–25] (together with their isomers pyrano[3,2-*a*]indolizin-2-ones)[25,26] (Fig. 1). However, their distinct structure, composed of a fused tricyclic system, in which a pyran ring is fused to an indolizine moiety, offers a wide range of opportunities for the design and development of novel compounds, exhibiting immense potential for applications in various fields, ranging from medicinal chemistry to materials science. Structurally, pyrano[2,3-*b*]indolizin-2-ones can be considered analogues of coumarins[27–34] and benzocoumarins.[35–42]

The synthesis of pyrano[2,3-*b*]indolizines was investigated by Kakehi and co-workers mainly from 1980 to 1998, driven by the need to establish an efficient and reliable methodology. Numerous synthetic routes have been explored, involving the use of pyridinium salts as starting materials and the formation of various intermediates, *e.g.* 3-bis(methylthio)methylene-2,3-dihydroindolizin-2-ones,[23] 2,3-dihydroindolizin-2-ones,[24] 3-vinylindolizines[25] as well as the hydrolysis of pyrano[2,3-*b*]indolizine-2-imines.[43] These synthetic efforts have resulted in the successful preparation of a diverse array of pyrano[2,3-*b*]

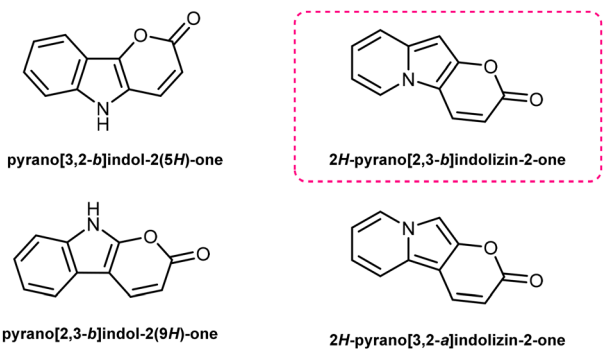

Fig. 1 Pyrano-indol-2-ones and pyrano-indolizin-2-ones.

[a]*Institute of Organic Chemistry, Polish Academy of Sciences, Kasprzaka 44/52, 01-224 Warsaw, Poland. E-mail: dtgryko@icho.edu.pl*
[b]*Nencki Institute of Experimental Biology, Polish Academy of Sciences, Pasteur 3, 02-093 Warsaw, Poland. E-mail: a.szewczyk@nencki.gov.pl*
[c]*Institute of Physics, Polish Academy of Sciences, Al. Lotników 32/46, 02-668 Warsaw, Poland. E-mail: deper@ifpan.edu.pl*

†Electronic supplementary information (ESI) available: NMR, UV/vis, fluorescence spectra and computational details. See DOI: https://doi.org/10.1039/d4qo01216j

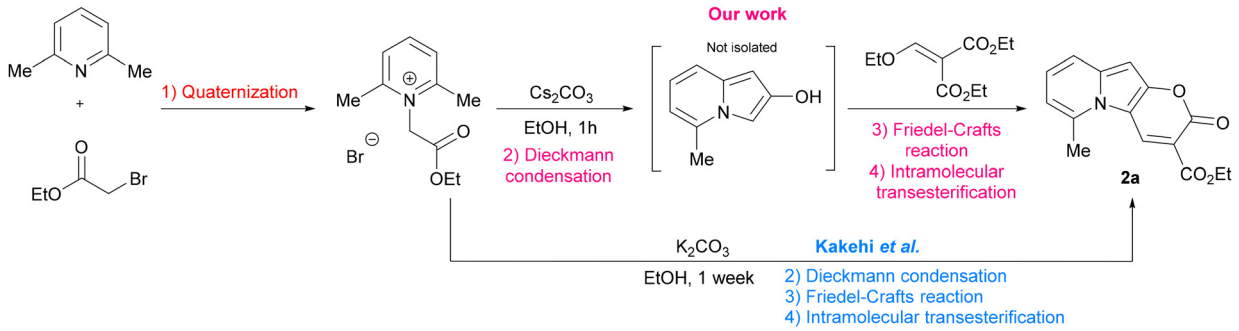

Scheme 1 Synthesis of ethyl 6-methyl-2-oxo-pyrano[2,3-*b*]indolizine-3-carboxylate.

indolizine derivatives, expanding the chemical space available for further exploration and application.

In the context of search for novel fluorescent platforms we resolved to explore 2-oxo-pyrano[2,3-*b*]indolizine-3-carboxylates because of the easily available starting materials and the strong fluorescence emission claimed by the authors in their paper, but not sufficiently explored.[24] The Kakehi's synthesis (Scheme 1) consisted of four steps: (1) quaternization of 2,6-dimethylpyridine with ethyl 2-bromoacetate; (2) Dieckmann condensation to form the 5-methylindolizin-2-ol intermediate; (3) Friedel–Crafts reaction of the intermediate with diethyl 2-(ethoxymethylene)malonate; (4) final intramolecular cyclization *via* transesterification with the formation of the lactone ring and additional ethanol elimination. It is noteworthy that the last three steps occur in one pot. However, the drawback of this methodology is that a long reaction time (7 days) is required, and the yield is relatively poor (38%). By solving the synthetic drawbacks and shedding light on the properties of this class of compounds, we aimed to provide a comprehensive understanding of this intriguing heterocyclic system, thus paving the way for further research and development of novel compounds with enhanced properties and biological application.

Results and discussion

Synthesis

Optimization. Our investigation started with the synthesis of the dye **2a** (Scheme 2), and we used this reaction as a model for the optimization studies, Table 1. First, we attempted to decrease the reaction time by changing the solvent to DMF (entry 2), but the expected product was not detected; instead, **2i** was obtained. Then we tried NaOEt as base (entry 3), but the product was observed only in trace amounts. At this point, before proceeding to test alternative bases, we hypothesized that sequential addition of reagents, allowing first the formation of the 5-methylindolizin-2-ol intermediate (Scheme 2) and then the following steps, could be the key to increasing the yield. Different bases were evaluated (entries 4–6) and we eventually found that the use of Cs_2CO_3 along with sequential addition of the reagents turned out to be pivotal to obtain a yield of 50% (entry 6). Interestingly, Cs_2CO_3 turned out to be the best base to promote the cyclization. This result can be partly attributed to the increased basicity strength *versus* that of K_2CO_3. And it is in line with some recently developed synthetic approaches.[44,45–47]

Scope. Having established the optimal reaction conditions (Cs_2CO_3, EtOH, RT, 18 h), the substrate scope was evaluated. As shown in Scheme 2, different 'formal' picolinium salts, prepared according to literature procedure (**1a–f**)[48–51] and used as such, reacted with Cs_2CO_3 to form the indolizin-2(3*H*)-one intermediate that, after addition of diethyl 2-(ethoxymethylene) malonate, successfully gave pyranoindolizines possessing a hydrogen or an alkyl substituent in position R^5 (**2a**, **2b**, **2c**) in 5–50% yield.

Consistent with what was observed by Kakehi and coworkers in 1986, the reaction with 2,3-cyclopentenopyridinium salts did not lead to the indolizine product,[52] while the reaction with a 5,6,7,8-tetrahydroquinolinium salt led to the expected product **2d** in 30% yield. 2-Methylquinolinium and 1-methylisoquinolinium salts also reacted nicely and gave π-expanded indolizine products with a free R^5 position (**2e**, **2f**) in 30 and 28% yield, respectively, while 3-methylisoquinolin-2-ium salt did not react as expected.

Additionally, α-picoline derivatives (**1g** and **1h**) bearing EWG groups (2-Py and CO_2Et) attached to the methylene group (R^5) furnished the target product (**2g**, **2h**) in 44% and 5% yield respectively. It is noteworthy that in those cases, due to the highly acidic character of the proton at the α-position, the quaternization of the pyridine with ethyl 2-bromoacetate led to a 3-substituted indolizin-2-ol directly, even in the absence of base. In such cases the base was added later, only to promote the last two steps: nucleophilic substitution and transesterification.

Meanwhile, the reaction from a 4-bromopyridinium salt and diethyl 2-(ethoxymethylene)malonate did not produce the expected product, probably due to a less reactive indolizin-2-ol intermediate. Similarly, the reaction with a 4-dimethylaminopyridinium salt did not give the target product, in this case probably due to the difficulty in the formation of the indolizine intermediate caused by the effect of the electron-donating group, which turned the proton in the α-position less acidic, thus the reagent is less prone to cyclization.

Functionalization. The structure of indolizine **2a** brings about exciting possibilities to create π-expanded, polarized

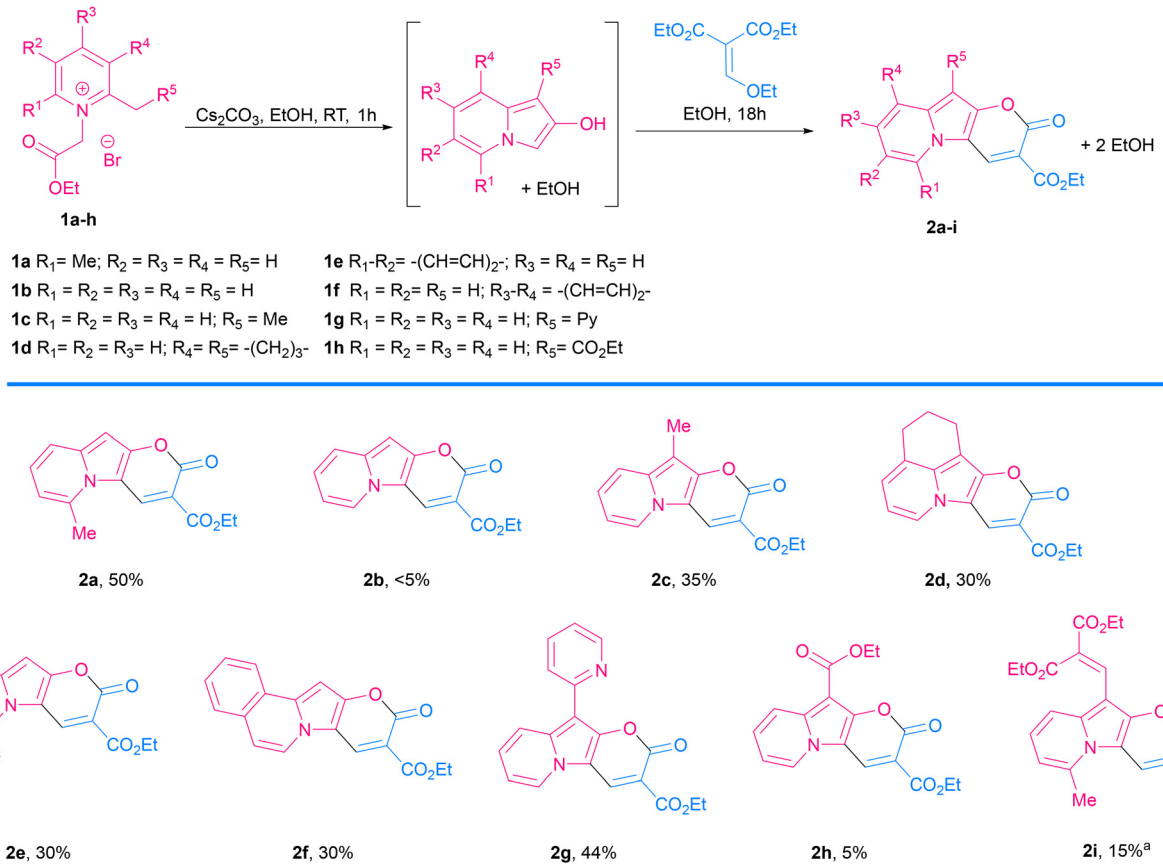

Scheme 2 Scope of 2-oxo-pyrano[2,3-*b*]indolizine-3-carboxylate. [a] Obtained by simultaneous addition of malonate.

Table 1 Conditions for the optimization of 6-methyl-2-oxo-pyrano[2,3-*b*]indolizine-3-carboxylate

Entry	Base	Solvent	*T*/°C	Time/h	Yield %
1[a]	K_2CO_3	EtOH	RT	7 days	38
2[b]	K_2CO_3	DMF	RT	18 h	15% of **2i**
3[b]	NaOEt	EtOH	RT	18 h	Traces
4[c]	KOH	EtOH	RT	18 h	30
5[c]	LiOH	EtOH	RT	18 h	15
6[c]	Cs_2CO_3	EtOH	RT	18 h	50

[a] Kakehi's methodology. [b] Simultaneous addition of malonate. [c] Postponed addition of malonate.

derivatives. Among a few possibilities, the presence of a highly electron-rich carbon β to the nitrogen was appealing to exploit (Scheme 3). To explore these possibilities, three additional derivatives (**3aa**, **3ab**, **3ac**) were obtained by direct arylation. As expected, bromoarenes with EWG in the *para* position, such as CN or NO_2, were more reactive in the direct arylation and the products were obtained in good yields (60% and 50%). In contrast, the bromoarene bearing an EDG, such as *t*Bu, gave the product **3ac** in poor yield (17%).

The Vilsmeier–Haack formylation also successfully occurred at the electron-rich position, resulting in the formation of **4a** in 83% yield.

To probe the potential of this class of dyes, Knoevenagel condensation was carried out between **4a** and 1,4-dimethylpyridin-1-ium iodide (**5**) (Scheme 3) forming a new styryl[53–55] dye **6a**, which was obtained in 37% yield and later evaluated for cell staining (*vide infra*).

Considering the principles of green chemistry,[56] the reactions leading to compounds **2a–2i** and **4a** are considered to have moderate atom economy (AE) efficiency, in the range of 40–60%. Meanwhile, direct arylation products (**3aa–3ac**) and Knoevenagel condensation were obtained with AE efficiency above 80%, which is considered optimal according to the above principles. For all reactions, the reaction mass efficiency is very low, less than 10%, mainly due to the significant impact of the solvent in the calculation.

Photophysical properties

UV-Vis absorption and emission spectra were recorded in non-polar toluene (dielectric constant ε = 2.38), moderately polar DCM (ε = 8.93), and polar DMSO (ε = 46.45) for all dyes, except **6a**, which was measured only in DCM and DMSO and will be discussed separately and correlated to its precursor **4a**.

A comparison between the photophysical parameters for 2-oxo-pyrano[2,3-*b*]indolizine-3-carboxylates and those available for similar structures (Fig. 2) such as 11-benzyl-7-hydroxyisochromeno[4,3-*b*]indol-5-one[9] (Φ_{fl} = 42% in DCM, with λ_{abs} =

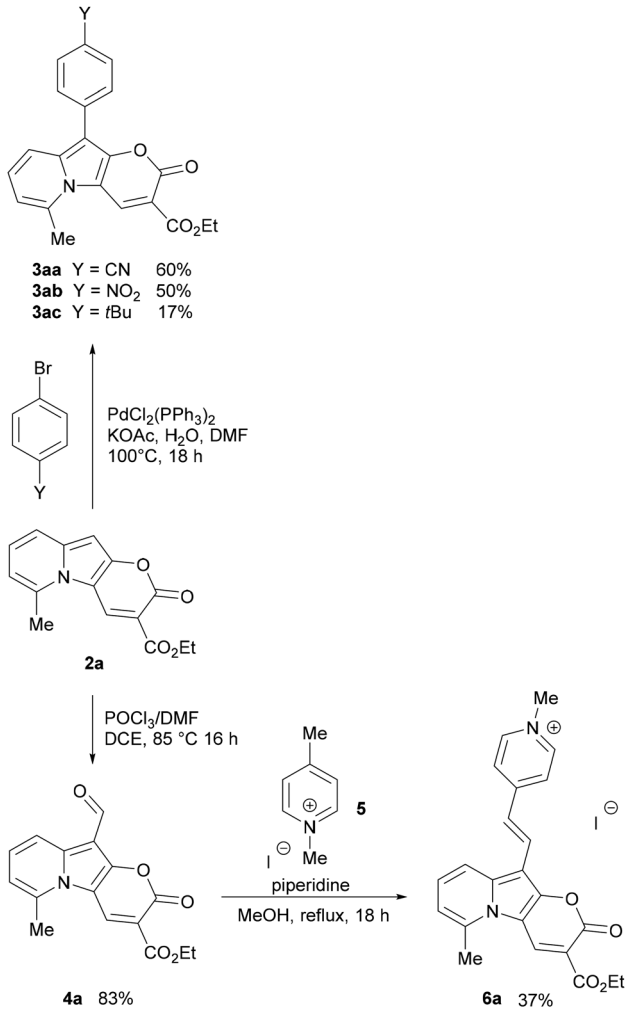

Scheme 3 Synthesis of **3aa**, **3ab**, **3ac** and **4a** from **2a**, and synthesis of **6a** from **4a**.

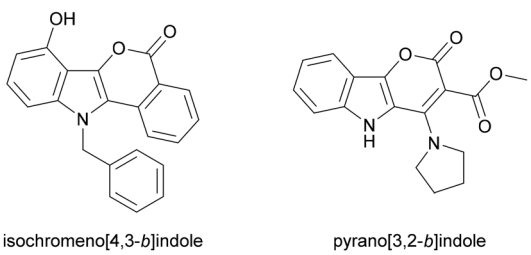

Fig. 2 Indoles structures used as reference to discuss photophysical properties of synthesized dyes.

382 and λ_{em} 496) or methyl 2-oxo-4-(pyrrolidin-1-yl)-2,5-dihydropyrano[3,2-*b*]indole-3-carboxylate[57] (λ_{abs} = 335 in EtOH) reveals a significant bathochromic shift for absorption, while emission and fluorescence quantum yield (Φ_{fl}) remain in the same range.

The collected data of compounds in DCM are presented in Table 2 and the spectra of selected dyes are compared in

Table 2 Photophysical data of synthesized 2-oxo-pyrano[2,3-*b*]indolizine derivatives in DCM

Cmp	Solv	λ_{abs} [nm]	λ_{em} [nm]	$\Delta\bar{\nu}$ [cm^{-1}]	ε [M^{-1} cm^{-1}]	Φ_{fl}
2a	DCM	446	464	900	30 500	0.71
2b	DCM	449	470	1000	16 300	0.77
2c	DCM	468	494	1100	22 900	0.61
2d	DCM	467	499	1400	24 600	0.64
2e	DCM	456	470	700	39 700	0.73
2f	DCM	436	458	1100	39 700	0.33
2g	DCM	466	500	1500	17 600	0.92
2h	DCM	433	452	1000	29 200	0.81
2i	DCM	446	485	1800	21 000	0.25
3aa	DCM	453	490	1700	22 928	0.64
3ab	DCM	452	491/642	6500	27 700	0.03
3ac	DCM	457	514	2400	19 600	0.65
4a	DCM	426	448	1200	31 800	0.77
6a[a]	DCM	509	575	2300	24 400	0.44

Fluorescence quantum yields measured with Coumarin 153 in EtOH as reference (Φ_{fl} = 0.55). [a] Fluorescence quantum yield measured with Rhodamine 6G in EtOH as reference (Φ_{fl} = 0.95).

Fig. 4, while the remaining data for the other solvents are available in Table S5 in ESI.† Absorption maxima (λ_{abs}) of the dyes obtained are located within 420–470 nm in all solvents, while the emission maxima (λ_{em}) falls between 440 and 520 nm for almost all of them and is more bathochromically shifted in polar solvents (solvatochromism). It is worth noting that compound **3ab** represents an exception to this trend in both DCM and DMSO, showing two emission bands overlapping, one at the 'expected' wavelength (491 nm) and another one around 642 nm. Excitation spectra were recorded to prove that both signals come from the same molecule and are not due to impurities in the sample. This property can be explained by hypothesizing that this structure, constituting of a strong donor, 2-oxo-pirano[2,3-*b*]indolizine, and a strong acceptor, nitrophenyl, can undergo internal charge transfer (ICT) in polar solvents and generate two possible excited states according to the geometry and consequently allow for two possible emitting paths.

The fluorescence quantum yields (Φ_{fl}) are in most cases on the same level regardless of the solvent and they vary among the studied 2-oxopyrano[3,2-*b*]indolizines from 0.92 for dye **2g** in DCM to being barely detectable for **3ab** in DCM and DMSO due to the preferred non-emissive decay (Fig. 3). Exceptions to this trend are **2c**, **2d**, **2g** that show lower fluorescence in toluene; and **3ab**, which shows a reverse trend by having the highest Φ_{fl} in the less polar solvent. The comparison of the photophysical properties of **2a**, **2b** and **2c** (Fig. 4A), which vary their position of a methyl group (or is absent), reveals that this alkyl group at position R^5 shifts both absorption and emission bathochromically (**2c** *vs.* **2b**) by about 20 nm, while the same group at position R^1 slightly shifts both signals hypsochromically (**2a** *vs.* **2b**).

Moreover, different electronic character of the substituent in R^5 (Fig. 4B) influences both λ_{abs} and λ_{em}. If CHO is present (**4a**), λ_{abs} = 426 nm and λ_{em} = 448 nm, while if Me is present (**2c**), λ_{abs} = 468 nm and λ_{em} = 494. The presence of a

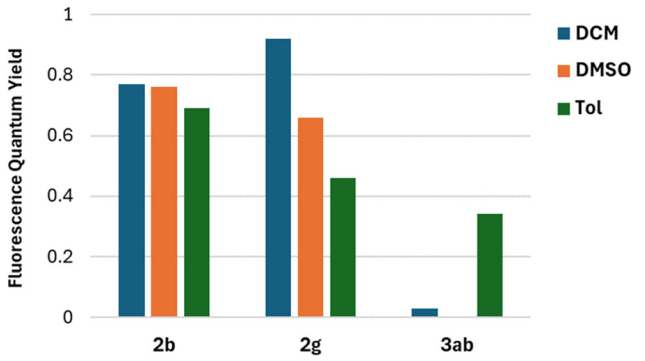

Fig. 3 Comparison of Fluorescence quantum yield in different solvents for representative compounds **2b**, **2g** and **3ab**.

π-extended system, as in **3aa** and **3ac**, slightly blue shifts the absorption. Additionally, having a *t*Bu group in the *para* position (**3ac**) red shifts the emission, consequently increasing the Stokes shift (2400 cm^{-1}). Interestingly, the effect of the π-expansion of the heterocyclic core strongly depends on the position of the fused benzene ring. In the case of dye **2f** a blue shift is observed accompanied with a decrease of the Φ_{fl} (0.33 *vs.* 0.77) compared to **2b** (Fig. 4C).

The addition of a methylpyridinium conjugated through an alkene to the 2-oxo-pirano[2,3-*b*]indolizine system (**6a**) allowed for an increased dipole moment that translates to a bathochromic shift of 83 nm for λ_{abs} and almost 130 nm for λ_{em} when compared to **4a** (Fig. 4D). Even though a decrease in the fluorescence quantum yield (0.44 *vs.* 0.77) was observed comparing **6a** and **4a**, the emission is still high suggesting that, in comparison to **3ab**, the decay through a radiative channel is favoured.

Fluorescence kinetic studies were performed for selected compounds: **2a** representing "typical" 2-oxo-pyrano[2,3-*b*]indolizine, **3ab** exhibiting dual fluorescence and salt **6a**. In all solvents fluorescence of dyes **2a** and **6a** decays exponentially (Fig. S11†) with decay times, τ_F, about 3.5 and 2.0 ns respectively (Table S6†). For both compounds τ_F changes slightly with solvent's polarity (represented by dielectric constant, ε) and the change is parallel to that of Φ_{fl}, – for **2a** both τ_F and Φ_{fl} grow with increasing ε whereas for **6a** they decrease (Table S6†). Consequently, the radiative rate constant $k_r = \Phi_{fl}/\tau_F$ of the $S_1 \rightarrow S_0$ transition remains constant and amounts to 1.3×10^8 s^{-1} and 2.1×10^8 s^{-1} respectively (Table S6†). Such high value is typical for the fully allowed ππ* transitions. For dye **3ab** kinetic traces are complex. In non-polar toluene fluorescence decays exponentially (Fig. S12a†) with characteristic time 2.62 ns (Table S7†). Radiative rate is 8.8×10^7 s^{-1}, much less than values obtained for dyes **2a** and **6a**. For polar solvents where dual fluorescence from LE and CT states is observed emission decays are non-exponential and depend on wavelength of observation. For DCM the high energy band of the LE state with maximum at 487 nm two components are clearly visible in the decay trace (Fig. S12b†), and deconvolution yields 20 and 356 ps decay times. Intensity of emission orig-

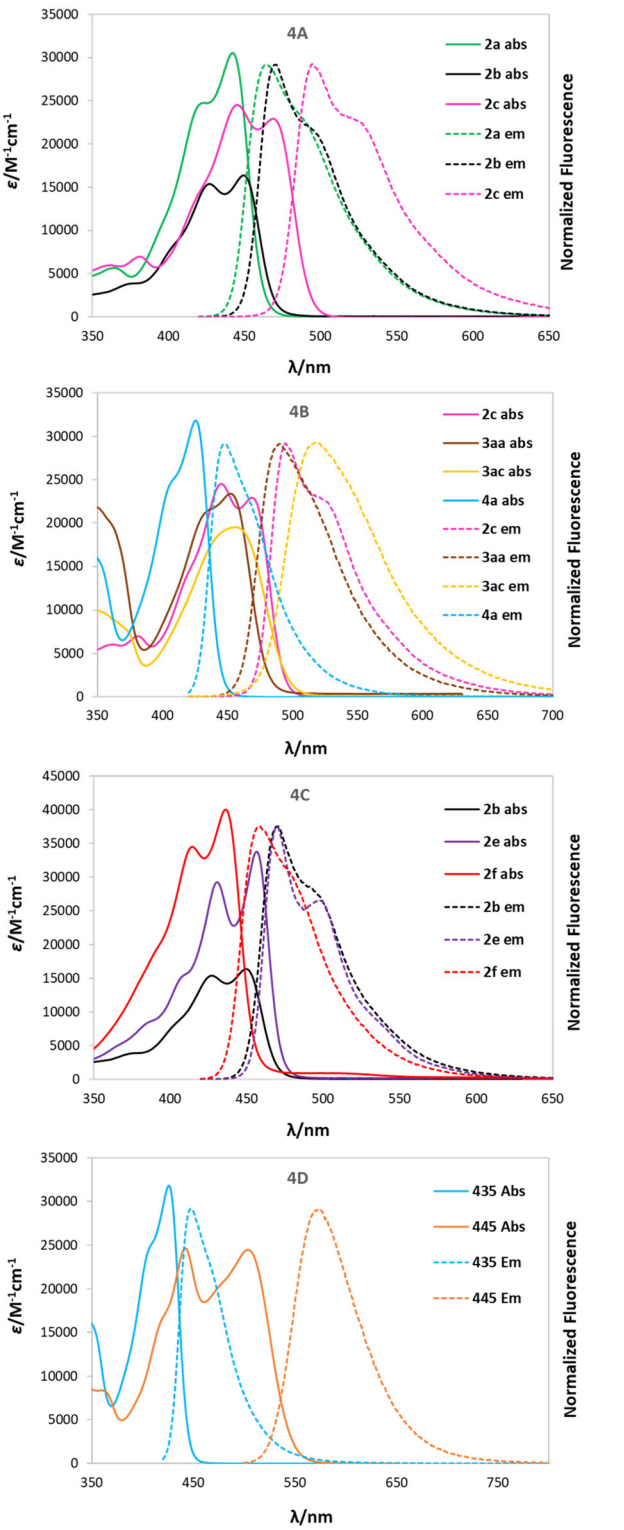

Fig. 4 Absorption and emission spectra of some representative 2-oxo-pyrano[2,3-*b*]indolizine-3-carboxylate derivatives in DCM. (A) Normalized absorption (solid line) and normalized emission (dashed line) of **2a**, **2b**, **2c** (green, black, pink) (B) normalized absorption (solid line) and normalized emission (dashed line) of **2c**, **3aa**, **3ac** and **4a** (pink, brown, yellow and light blue) (C) normalized absorption (solid line) and normalized emission (dashed line) of **2b**, **2e** and **2f** (black, purple, red) (D) normalized absorption (solid line) and normalized emission (dashed line) of **4a** and **6a** (light blue, orange).

inating from low energy CT band with maximum at 700 nm grows at early times and reaches maximum much later than the LE profile (Fig. S12b†). This points to precursor (LE) – successor (CT) scheme and suggests that that initial population of the CT state is null. Indeed, deconvolution reveals grow time of 55 ps and decay time of 356 ps (Table S7†). Negative amplitude of the grow time is comparable to the (positive) amplitude of the decay time what confirms that CT state is not directly excited and is populated from the LE state. This provides experimental proof for the TICT concept hypothesised below. Long component of the LE profile has same decay time as decay time of CT trace, pointing to thermalization of both states. However, grow time of CT is a bit longer than the short decay time of LE so one may expect presence of a transition state or a slow relaxation to emissive CT structure, so the simple two states model used commonly for TICT can be not adequate. In more polar DMSO kinetic profiles are faster (Fig. S12c†) and the LE decay time decreases down to 15 ps (Table S7†) pointing to the increase of the intramolecular CT rate constant. Formation of TICT enhances also non-radiative relaxation, hence the Φ_{fl} decreases by two orders of magnitude.

Theoretical analysis

The DFT and TDDFT O3LYP/6-31G(d,p) calculations were performed to corroborate the experimental data. The choice of the O3LYP functional allows for the best reconstruction of the spectral data in comparison to our attempts using other functionals (Table S1†). Calculations included the optimization of molecular structures in their ground (S_0) and lowest electronic excited (S_1) states along with the determination of the corresponding absorption and fluorescence energies. Corresponding data for the molecules in the three solvents, toluene, DCM and DMSO, are collected in Table S2.† The calculated dipole moments for the S_0 and S_1 states are summarized in Table S3.† The two highest occupied (HOMO's) and two lowest unoccupied molecular orbital (LUMO's) energy levels are shown in the diagram in Fig. S1,† while the values of HOMO and LUMO energies are given and compared in Table S4.† More detailed results of calculations are in the ESI.†

Dye **2b** lacking any substituents can be considered a model chromophore for this family of heterocycles (Scheme 2). This is a molecule with planar geometry in both S_0, and S_1, states. The electronic transition between them has a π–π^* character and essentially it is described by a single HOMO/LUMO electronic configuration. A diagram of the calculated electronic states of heterocycle **2b** with a short analysis is presented in ESI, Fig. S2.†

According to the computational results, the geometry of **2b** in the excited state undergoes relatively small changes. This result is consistent with the small Stokes shift observed experimentally. Small changes in geometry are manifested by small Franck–Condon factors (Fig. S3†) which well reproduce the experimental spectrum (Fig. 1). The small values of the calculated spin–orbit coupling elements (H_{so}) between the excited S_1 state and the energetically close triplet states (Fig. S2†) together with the small Franck–Condon factors are indicative of relatively small rate constants of non-radiative processes,[58,59] which in the experiment (Table 2) is visible as significant values of Φ_{fl} achieved for dye **2b**.

The calculation results show also, that **2b** is a molecule with a large dipole moment, increasing in the excited state (9.6 D for S_0 state and 12 D in S_1 – Table S3†). In this light, slight red-shifts of its electronic spectra (both observed, Table 2 and Table S5† and calculated, Table S2†) as the solvent polarity increases may seem surprisingly small. This phenomenon, has also been observed in the case of various other molecules,[60,61] and can be explained with the use of classical theory of the solvent effect,[60,61] and is related to the fact that dipole moments are vector quantities (and not scalars). When the increase in the dipole moment in the S_1 state (relative to the S_0 state) is accompanied by a change of orientation in space, the solvent effect is smaller than expected based on values alone (see Fig. S4†).

Fig. S2† shows the shapes of the HOMO and LUMO of molecule **2b**, providing high oscillator strength for the transition between the S_0 and S_1 states. They will constitute a reference orbital in the presentation of results for other 2-oxopyrano[3,2-*b*]indolizines.

The substitution of molecule **2b** causes changes in the energy of the molecular orbitals (Fig. S1†), including changes in the spacing between them (Table S4†). This is reflected by the shifts of the electronic spectra, since the electronic transition has an initial and final state, the magnitude of this shift depends on the energy changes in both states.

In Fig. 5, correlation between the absorption $S_0 \rightarrow S_1$ energy and the energy difference of the HOMO and LUMO for the studied 2-oxopyrano[2,3-*b*]indolizines is presented. This correlation demonstrates that transitions between the S_0 and S_1 states for all molecules, as in parent dye **2b**, are described by a single HOMO/LUMO electronic configuration. At the same

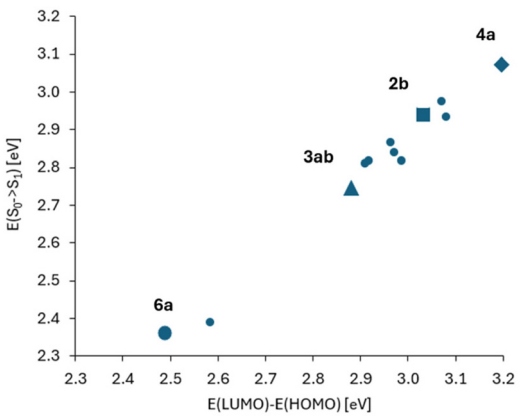

Fig. 5 Correlation between the absorption energy and the energy difference of HOMO and LUMO orbitals (numerical data in Tables S2 and S4†). The point corresponding to molecule **2b** is marked with a square. Two distant points (for lower energies, *i.e.* with red shift in comparison to **2b**) correspond to molecules **3ab** and **6a**. These two molecules also differ from the others in large values and changes of the dipole moment between S_0 and S_1 states (Table S3†).

time, two groups of molecules can be distinguished, the first with moderate changes in the HOMO/LUMO energy gaps and excitation energies (in relation to **2b**), and the other group of two molecules with large changes in these quantities.

Fig. 6 (part of the diagram in Fig. S1†) illustrates the variation of the *E*(HOMO)–*E*(LUMO) gap and shows the shapes of these orbitals for four representatives of the studied family of 2-oxopyrano[2,3-*b*]indolizines: **2b** – as a model chromophore, **3ac** – a dye with observed red-shift in the absorption and fluorescence spectra (relative to the spectra of **2b**), **4a** – with a blue-shift of the spectra and dye **6a** – as a molecule with large red-shift of electronic spectra (see also Fig. 4).

Based on Fig. 6, it can be concluded that the effect of substitution of molecule **2b** produces two qualitatively different effects depending on the electron affinity of the substituent. In the case of compounds **3ac** and **4a**, this is a modification effect, *i.e.* their HOMO and LUMO are the modified (to a larger or smaller extent) HOMO and LUMO of molecule **2b**, but this is no longer the case of the LUMO of molecule **6a**. Although the HOMO of **6a** is still a modified HOMO of molecule **2b**, the LUMO is the orbital located on the substituent (while the orbital located on core **2b** lies above it, as shown in Fig. 6).

In addition to the diagram shown on Fig. 6, two other diagrams are shown in the ESI (Fig. S5 and S6†): HOMO/LUMO energy changes from methylation of the dye **2b** in different positions (**2a** *vs.* **2c**) and with π-extension (**2e** *vs.* **2f**) of **2b**. Methylation of **2b** at the R^5 position causes the largest change in HOMO energy leading to a red shift of the **2c** spectra.

In contrast to the substitution with a single bond, the π-expansion of **2b** becomes a problem not only at the level of the HOMOs, but also at the level of the (so far untouched) LUMO of molecule **2b**.

Therefore, the reason for the large red shift of the **6a** (and **3ab**) spectra is a qualitative change of LUMO from localized on **2b** to localized on the substituent. The $S_0 \rightarrow S_1$ transition becomes, instead of the modified **2b** excitation, intramolecular charge-transfer between the core and the substituent.

Both orbitals are extended into the attached ring. The energy effect depends on the geometry in which the expansion is carried out (E_{LUMO}(**2e**) < E_{LUMO}(**2f**)).

The calculation results for excited states indicate that most of the considered molecules retain features characteristic of parent dye **2b**. The fluorescence energies of the molecules optimized in the excited state are not very far from the absorption energies, and these transitions are described by high oscillator strengths (Table S1†). Although these results are in agreement with the experiments, (small Stokes shift, large emission efficiencies) these facts may seem surprising at first. This is because in these dyes there is a convenient relaxation path, which is a rotation around a single bond connecting the substituents with the heterocyclic core **2b**. We can expect two effects to play a role: a difference between the dihedral angles corresponding to the energy minimum in the ground and excited states, as well as the formation of rotational conformers. Differences between geometries optimized in the ground and excited states do indeed exist. For example, in systems containing a phenyl substituent at position R^5, such as **3aa**, in the ground state, the aromatic ring makes an angle of 41.3° with the **2b** plane, while in the optimized excited state it makes an angle of 30.7°; a similar rotation occurs in **3ac**, from 35.9° to 29.5°. However, they do not have a major impact on the spectroscopic properties because the LUMO is not extended to the substituent (Fig. 6). The exceptions are two molecules: **3ab** and **6a**, because their LUMOs are located on the substituent (Fig. 6, S7 and S8†). In both cases, the dark rotational conformers were optimised in the excited state (Table S1†). These conformers are characterised by zero oscillator strength for $S_1 \rightarrow S_0$ transition at the perpendicular arrangement of the planes of the heterocyclic core and the substituent ring. The difference between **6a** and **3ab** is that the dark form of **3ab** is the only form optimized in the excited state in polar DMSO. This result is consistent with experimental: while **6a** in this solvent emits with significant efficiency, the emission yield of **3ab** is extremely low. This means that the relaxation of **6a** to the dark state is slower than the decay *via* the radiative channel or inhibited by a barrier due to a more complex link between substituent and the heterocyclic core.

In turn, the bright form of **3ab** is experimentally observed and optimised in calculations for the S_1 state, in a non-polar medium only. Fig. S8† shows a diagram of electronic states of isolated molecule **3ab** with both optimised forms of the excited state. This is a diagram typical of TICT systems.[62]

Overall, it is worth to acknowledge the consistency between experimental and theoretical results. The ratio of radiative rate constant of **2a** and **6a**, 1.3/2.1 = 0.62 is very similar to the ratio

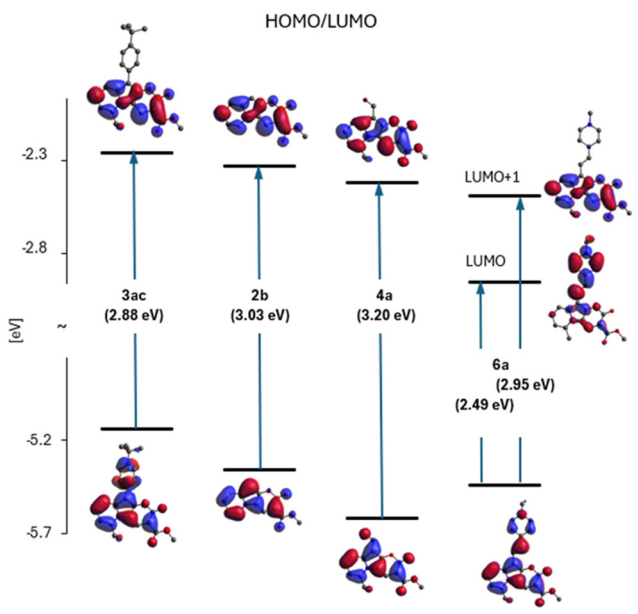

Fig. 6 Diagram of orbital energies: **2b** as the model heterocycle and its three derivatives, **3ac**, **4a** and **6a** in DMSO. The numbers in brackets indicate the size of the HOMO/LUMO energy gaps. In the case of **6a** two LUMOs are present in the considered energy region and in contrary to previous cases lowest of them is localised on substituent.

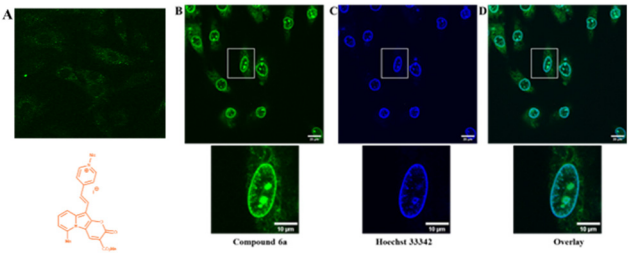

Fig. 7 Intracellular localization of compound **6a** in H9c2 cells detected using confocal fluorescence microscopy. (A) Image of the cells incubated with dye **6a** in a non-permeabilized cell membrane. Lower diagram structure of the dye. (B) Fluorescence of cells with digitonin (100 μg ml^{-1}) permeabilized membrane. (C) Fluorescence of permeabilized cell co-incubated with 0.5 μM Hoechst 33342 recorded with a 405 nm excitation wavelength and emission ranges from 420–520 nm. (D) Overlay of B and C. Lower pictures represents zoom upper square marked cells for B, C and D. The fluorescence of **6a** was recorded with a 473 nm excitation wavelength and emission ranges from 510–610 nm.

oscillator strength calculated for them, 0.64 : 1.06 (Tables S1 and S7†). Also, the radiative rate obtained experimentally for **3ab** is two/three times lower than for **2a**/**6a**, exactly like the oscillator strength calculated for **3ab** and **2a**/**6a** (Tables S1 and S7†). For **3ab** the theoretically predicted TICT mechanism is fully confirmed by fluorescence kinetic study. These as well as other correspondence between theory and experiment supports confidence for the HOMO and LUMO overlap statements.

Imaging studies

To prove the potential applicability of 2-oxo-pyrano[2,3-*b*]indolizines as a fluorescent probes, incubation of rat embryonic cardiomyoblast-derived cells H9c2 with selected dyes **2g**, **2c**, **4a** and **6a** was performed. The results showed that, neutral dyes from this family (*i.e.* **2g**, **2c** and **4a**) penetrate the living cell membrane and, as they are uncharged, accumulate nonspecifically in a wide range of cellular structures (Fig. S13†). In the case of dye **6a** which is a quaternary pyridinium salt, imaging experiments did not lead to accumulation of the dye intracellularly (Fig. 7A). To promote the access to the cytosol, H9c2 were permeabilized with digitonin (100 μg ml^{-1}). Addition of digitonin to the incubation medium resulted in permeabilization of the cell membrane and the successful penetration of the dye into the cytosol and cell organelles (Fig. 7B). It turned out that under these conditions, compound **6a**, as seen in the presented image (Fig. 7B), the dye was accumulated in the structure of the nucleus and the nuclear membrane. In order to compare the dye **6a** with the classical cell nuclear stain, co-staining with Hoechst 33342 was performed (Fig. 7C). It appears that the fluorescence of these two dyes overlaps except for some intranuclear structures, which are more strongly stained by pyranoindolizine **6a** (Fig. 7C and D). Additional intranuclear structures more strongly stained by the dye **6a** may prove useful in distinguishing specific cell nuclear structures.

Conclusions

In conclusion, the synthesis of pyrano[2,3-*b*]indolizin-2-ones from picolinium salts and diethyl 2-(ethoxymethylene) malonate under basic conditions could be optimized to reach 50% yields for the one-pot procedure. The presence of an electron-rich pyrrolic position can be harnessed to open the avenue towards various novel derivatives. The presence of different substituents on the starting picoline as well as post-functionalization allowed for detailed studies on their impact on the photophysical properties in polar and non-polar solvents. It was found that the fluorescence intensity is large for all studied pyrano[2,3-*b*]indolizin-2-ones regardless of the substitution pattern which originates from the almost complete overlap of the HOMO and LUMO. Combined experimental and computational study enabled to conclude that pyrano[2,3-*b*]indolizin-2-one core can be considered as an electron-acceptor and in most of the derivatives examined in this work, the consequence of π-expansion was the extension of the HOMO and the modification of the electronic transition energy in the range of 0.2 eV. We discovered that a simultaneous increase in the dipole moment and change of its orientation in space is the reason for maintaining the large emission intensity as well as the small Stokes shift and solvatochromism, in polar solvents. Studies on the staining of the H9c2 cell line with exemplary 2-oxo-pyrano[2,3-*b*]indolizines has proven that uncharged dyes easily penetrate the living cells' membrane. On the other hand styryl derivative **6a** does not, it specifically stains structures associated with the cell nucleus of permeabilized cells. All reported findings may serve as the guide enabling modulation of this class of molecules towards the design of improved dyes for cell imaging applications.

Experimental section

General synthetic information

All reagents and solvents were purchased from commercial sources and used as received. Reactions with moisture and oxygen sensitive compounds were performed under an argon atmosphere. The progress of reactions was monitored by thin-layer chromatography (TLC), performed on aluminum foil plates, covered with silica gel 60 F_{254} (Merck). Pure products were achieved by means of column chromatography with silica gel 60 (230–400 mesh). The identity and purity of final products were established by ^{1}H and ^{13}C NMR spectrometry as well as by MS-spectrometry (APCI-MS or ESI-MS). All reported ^{1}H NMR and ^{13}C NMR spectra were recorded on Varian AM 500 MHz, or Varian AM 600 MHz spectrometers. Chemical shifts (ppm) were determined with TMS as internal reference; *J* values are given in Hz. All melting points were measured with EZ-Melt apparatus.

Synthesis of precursors for pyrano[2,3-*b*]indolizin-2-ones

Pyridinium salts **1a**,[48] **1b**,[49] **1c**,[50] **1d**,[48] **1e**,[51] **1f**,[50] and bis(2-pyridyl)methane **0g**[63] were synthesized according to previously published procedures, and spectroscopic data are consistent.

1-(2-Ethoxy-2-oxoethyl)-2,6-dimethylpyridin-1-ium bromide (1a). ^{1}H NMR (600 MHz, DMSO-d_6) δ 8.46 (t, J = 7.9 Hz, 1H), 7.99 (d, J = 7.9 Hz, 2H), 5.62 (s, 2H), 4.26 (q, J = 7.1 Hz, 2H), 2.78 (s, 6H), 1.25 (t, J = 7.1 Hz, 3H).

1-(2-Ethoxy-2-oxoethyl)-2-methylpyridin-1-ium bromide (1b). ^{1}H NMR (600 MHz, DMSO-d_6) δ 9.01 (dd, J = 6.2, 1.3 Hz, 1H), 8.61 (td, J = 7.8, 1.5 Hz, 1H), 8.15 (d, J = 7.9 Hz, 1H), 8.08 (ddd, J = 7.7, 6.0, 1.5 Hz, 1H), 5.73 (s, 2H), 4.26 (q, J = 7.1 Hz, 2H), 2.77 (s, 3H), 1.26 (t, J = 7.1 Hz, 3H).

1-(2-Ethoxy-2-oxoethyl)-2-ethylpyridin-1-ium bromide (1c). ^{1}H NMR (600 MHz, DMSO-d_6) δ 9.07 (d, J = 5.4, Hz, 1H), 8.65 (td, J = 7.9, 1.5 Hz, 1H), 8.15 (d, J = 7.9 Hz, 1H), 8.11–8.07 (m, 1H), 5.78 (s, 2H), 4.23 (q, J = 7.1 Hz, 2H), 3.05 (q, J = 7.4 Hz, 2H), 1.28 (t, J = 7.4 Hz, 3H), 1.24 (t, J = 7.1 Hz, 3H).

1-(2-Ethoxy-2-oxoethyl)-5,6,7,8-tetrahydroquinolin-1-ium bromide (1d). ^{1}H NMR (500 MHz, DMSO-d_6) δ 8.90 (d, J = 6.1 Hz, 1H), 8.42 (d, J = 7.9 Hz, 1H), 7.97 (dd, J = 7.9, 6.2 Hz, 1H), 5.70 (s, 2H), 4.23 (q, J = 7.1 Hz, 2H), 3.00–2.97 (m, 4H), 1.90–1.84 (m, 2H), 1.76–1.70 (m, 2H), 1.23 (t, J = 7.1 Hz, 3H).

1-(2-Ethoxy-2-oxoethyl)-2-methylquinolin-1-ium bromide (1e). ^{1}H NMR (600 MHz, DMSO-d_6) δ 9.31 (d, J = 8.5 Hz, 1H), 8.48–8.50 (m, 2H), 8.30–8.23 (m, 2H), 8.03 (t, J = 7.5 Hz, 1H), 6.12 (s, 2H), 4.28 (q, J = 7.1 Hz, 2H), 3.12 (s, 3H), 1.27 (t, J = 7.1 Hz, 3H).

2-(2-Ethoxy-2-oxoethyl)-1-methylisoquinolin-2-ium bromide (1f). ^{1}H NMR (500 MHz, DMSO-d_6) δ 8.80 (d, J = 8.8, 1H), 8.70 (d, J = 6.9 Hz, 1H), 8.49 (d, J = 6.9 Hz, 1H), 8.33 (d, J = 8.1 Hz, 1H), 8.27 (dd, J = 7.5, 7.5 Hz, 1H), 8.08 (ddd, J = 8.4, 6.8, 1.3 Hz, 1H), 5.91 (s, 2H), 4.25 (q, J = 7.1 Hz, 2H), 3.21 (s, 3H), 1.25 (t, J = 7.1 Hz, 3H).

1-(Pyridin-2-yl)indolizin-2-ol (1g). In a round bottom flask, bis(2-pyridyl)methane (1.70 g, 10 mmol) was mixed with ethyl 2-bromoacetate (1.11 mL, 10 mmol) in ethanol and heated at 60 °C overnight. The pyridinium salt was not possible to isolate since the reaction spontaneously proceeded to the cyclization. After confirming the formation of the indolizine on TLC with Ehrlich's reagent, the solvent was evaporated, and the crude was used for the next reaction.

Ethyl 2-oxo-2,3-dihydroindolizine-1-carboxylate (1h). In a round bottom flask, ethyl 2-(pyridyn-2-yl)acetate (1.61 mL, 10 mmol) was mixed with ethyl 2-bromoacetate (1.11 mL, 10 mmol) in ethanol and heated at 60 °C overnight. The pyridinium salt was not possible to isolate since the reaction spontaneously proceeded to the cyclization. After confirming the formation of the indolizine on TLC with Ehrlich's reagent, solvent was evaporated, and the crude was used for the next reaction.

Di(pyridin-2-yl)methane (0g). ^{1}H NMR (600 MHz, DMSO-d_6) δ 8.45 (ddd, J = 4.9, 1.9, 0.9 Hz, 2H), 7.64 (td, J = 7.6, 1.9 Hz, 2H), 7.26 (dt, J = 7.9, 1.2 Hz, 2H), 7.16 (ddd, J = 7.7, 4.9, 1.2 Hz, 2H), 4.23 (s, 2H).

General procedure for the synthesis of 2-oxo-2*H*-pyrano[2,3-*b*]indolizine-3-carboxylates (condition A)

In a 20 mL Schlenk flask, pyridinium salt (6 mmol, 1 equiv.) and Cs_2CO_3 (6 mmol, 1 equiv.) were added and dissolved in 5 mL of ethanol. After 1–2 hours a color change in the mixture was observed and fluorescence, typical for indoles, was visible when irradiated with UV lamp. Diethyl 2-(ethoxymethylene) malonate (6 mmol, 1 equiv.) was added, and the reaction mixture was stirred overnight at room temperature. After completion, the mixture was extracted with DCM, and the combined organic layers were dried over Na_2SO_4 and concentrated under reduced pressure. The crude product was purified by column chromatography (silica, AcOEt/hexane 1 : 1).

Ethyl 6-methyl-2-oxo-2*H*-pyrano[2,3-*b*]indolizine-3-carboxylate (2a). According to the general procedure **(condition A)**, 1-(2-ethoxy-2-oxoethyl)-2,6-dimethylpyridin-1-ium bromide (500 mg, 1.82 mmol), Cs_2CO_3 (594 mg, 1.82 mmol) and diethyl 2-(ethoxymethylene)malonate (0.369 mL, 1.82 mmol) were reacted affording **2a** (250 mg, 50%) as yellow/orange crystals. R_f = 0.48 (SiO_2, AcOEt/hexane, 3 : 1); m.p. 189.0 °C. ^{1}H NMR (500 MHz, $CDCl_3$) δ 8.97 (s, 1H), 7.46 (d, J = 8.8 Hz, 1H), 7.25 (dd, J = 8.8, 7.0 Hz, 1H), 6.77 (d, J = 7.0 Hz, 1H), 6.43 (s, 1H), 4.41 (q, J = 7.1 Hz, 2H), 2.89 (s, 3H), 1.41 (t, J = 7.1 Hz, 3H). ^{13}C NMR (126 MHz, $CDCl_3$) δ 165.8, 158.3, 153.7, 142.1, 138.4, 138.1, 126.9, 117.0, 114.5, 112.7, 100.8, 89.0, 61.2, 22.0, 14.5 ppm. HRMS (ESI): m/z calcd for $C_{15}H_{13}NO_4Na$, 294.0742 $[M + Na]^+$; found, 294.0741.

Ethyl 2-oxo-2*H*-pyrano[2,3-*b*]indolizine-3-carboxylate (2b). According to the general procedure **(condition A)**, 1-(2-ethoxy-2-oxoethyl)-2-methylpyridin-1-ium bromide (0.500 mg, 2.77 mmol), Cs_2CO_3 (904 mg, 2.77 mmol) and diethyl 2-(ethoxymethylene)malonate (0.561 mL, 2.77 mmol) were reacted affording **2b** (20 mg, 5%) as yellow crystals. R_f = 0.32 (SiO_2, AcOEt/hexane, 3 : 1); m.p. 199.5 °C. ^{1}H NMR (500 MHz, $CDCl_3$) δ 8.81 (s, 1H), 8.27 (d, J = 6.9 Hz, 1H), 7.50 (d, J = 9.0 Hz, 1H), 7.26–7.20 (m, 1H), 6.90 (t, J = 6.9 Hz, 1H), 6.33 (s, 1H), 4.41 (q, J = 7.1 Hz, 2H), 1.41 (t, J = 7.1 Hz, 3H). ^{13}C NMR (126 MHz, $CDCl_3$) δ 165.1, 158.8, 152.9, 140.5, 133.7, 126.3, 124.6, 119.4, 113.0, 111.2, 101.9, 88.2, 61.3, 14.5. HRMS (ESI): m/z calcd for $C_{14}H_{11}NO_4Na$, 280.0586 $[M + Na]^+$; found, 280.0583.

Ethyl 10-methyl-2-oxo-2*H*-pyrano[2,3-*b*]indolizine-3-carboxylate (2c). According to the general procedure **(condition A)**, 1-(2-ethoxy-2-oxoethyl)-2-ethylpyridin-1-ium bromide (0.200 mg, 1.03 mmol), Cs_2CO_3 (335 mg, 1.03 mmol) and diethyl 2-(ethoxymethylene)malonate (0.208 mL, 1.03 mmol) were reacted affording **2c** (100 mg, 35%) as orange crystals. R_f = 0.54 (SiO_2, AcOEt/hexane, 3 : 1); m.p. 215.8 °C. ^{1}H NMR (500 MHz, $CDCl_3$) δ 8.76 (s, 1H), 8.23 (dt, J = 6.9, 1.1 Hz, 1H), 7.45 (dt, J = 9.0, 1.2 Hz, 1H), 7.21 (ddd, J = 9.0, 6.8, 1.1 Hz, 1H), 6.86 (td, J = 6.9, 1.2 Hz, 1H), 4.40 (q, J = 7.1 Hz, 2H), 2.30 (s, 3H), 1.41 (t, J = 7.1 Hz, 3H). ^{13}C NMR (126 MHz, $CDCl_3$) δ 165.3, 159.2, 150.7, 139.7, 133.1, 125.6, 124.5, 117.5, 112.6, 110.8, 100.8, 96.6, 61.1, 14.5, 6.2 ppm. HRMS (ESI): m/z calcd for $C_{15}H_{13}NO_4Na$, 294.0742 $[M + Na]^+$; found, 294.0739.

Ethyl 8-oxo-5,6-dihydro-4*H*,8*H*-pyrano[2′,3′:4,5]pyrrolo[3,2,1-*ij*]quinoline-9-carboxylate (2d). According to the general procedure **(condition A)**, 1-(2-ethoxy-2-oxoethyl)-5,6,7,8-tetrahydroquinolin-1-ium bromide (250 mg, 1.13 mmol), Cs_2CO_3 (370 mg, 1.13 mmol) and diethyl 2 (ethoxymethylene)malonate (0.229 mL, 1.13 mmol) were reacted affording **2d** (110 mg, 30%) as orange/red crystals. R_f = 0.48 (SiO_2, AcOEt/hexane, 3 : 1); m.p. 244.1 °C. ^{1}H NMR (600 MHz, $CDCl_3$) δ 8.76 (s, 1H), 8.05 (dd, J = 6.9, 0.8 Hz, 1H), 6.90 (dd, J = 6.9, 0.8 Hz, 1H), 6.79 (t, J = 6.8 Hz, 1H), 4.40 (q, J = 7.1 Hz, 2H), 2.93–2.86 (m, 4H), 2.03 (p, J = 6.1 Hz, 2H), 1.41 (t, J = 7.1 Hz, 3H). ^{13}C NMR (151 MHz, $CDCl_3$) δ 165.4, 159.3, 148.0, 139.5, 133.6, 130.8, 121.8, 121.5, 113.4, 111.5, 99.9, 98.3, 61.1, 27.4, 22.0, 19.8, 14.5 ppm. HRMS (ESI): m/z calcd for $C_{17}H_{15}NO_4Na$, 320.0899 $[M + Na]^+$; found, 320.0902.

Ethyl 9-oxo-9*H*-pyrano[2′,3′:4,5]pyrrolo[1,2-*a*]quinoline-10-carboxylate (2e). According to the general procedure **(condition A)**, 1-(2-ethoxy-2-oxoethyl)-2-methylquinolin-1-ium bromide (200 mg, 0.645 mmol), Cs_2CO_3 (210 mg, 0.645 mmol) and diethyl 2-(ethoxymethylene)malonate (0.130 mL, 0.645 mmol) were reacted affording **2e** (60 mg, 30%) as yellow crystals. R_f = 0.56 (SiO_2, AcOEt/hexane, 2 : 1); m.p. not measured, decomposed around 280 °C. ^{1}H NMR (500 MHz, $CDCl_3$) δ 9.36 (s, 1H), 8.32 (d, J = 8.5 Hz, 1H), 7.82 (dd, J = 7.9, 1.3 Hz, 1H), 7.77–7.72 (m, 1H), 7.54–7.48 (m, 2H), 7.41 (d, J = 9.2 Hz, 1H), 6.48 (s, 1H), 4.46 (q, J = 7.1 Hz, 2H), 1.45 (t, J = 7.1 Hz, 3H). ^{13}C NMR (126 MHz, $CDCl_3$) δ 165.5, 157.9, 154.3, 140.0, 138.0, 134.6, 130.6, 130.1, 127.8, 125.1, 124.3, 117.8, 115.6, 114.2, 103.5, 91.7, 61.6, 14.5 ppm. HRMS (APCI): m/z calcd for $C_{18}H_{13}NO_4$, 307.0845 [M−]; found, 307.0847.

Ethyl 10-oxo-10*H*-pyrano[2′,3′:4,5]pyrrolo[2,1-*a*]isoquinoline-9-carboxylate (2f). According to the general procedure **(condition A)**, 2-(2-ethoxy-2-oxoethyl)-1-methylisoquinolin-2-ium bromide (250 mg, 0.806 mmol), Cs_2CO_3 (263 mg, 0.806 mmol) and diethyl 2-(ethoxymethylene)malonate (0.163 mL, 0.806 mmol) were reacted affording **2f** (70 mg, 28%) as yellow crystals. R_f = 0.64 (SiO_2, AcOEt/hexane, 3 : 1); m.p. 261.2 °C. ^{1}H NMR (600 MHz, $CDCl_3$) δ 8.79 (d, J = 0.8 Hz, 1H), 8.11–8.08 (m, 1H), 8.01 (d, J = 7.1 Hz, 1H), 7.74–7.69 (m, 1H), 7.65–7.58 (m, 2H), 7.11 (d, J = 7.2 Hz, 1H), 6.84 (s, 1H), 4.41 (q, J = 7.1 Hz, 2H), 1.41 (t, J = 7.1 Hz, 3H). ^{13}C NMR (151 MHz, $CDCl_3$) δ 165.0, 158.8, 152.9, 138.6, 134.0, 129.6, 129.2, 128.7, 127.6, 124.3, 121.0, 113.2, 112.5, 103.3, 88.8, 61.4, 14.4 ppm. HRMS (ESI): m/z calcd for $C_{18}H_{13}NO_4Na$, 330.0742 $[M + Na]^+$; found, 330.0746.

Ethyl 2-oxo-10-(pyridin-2-yl)-2*H*-pyrano[2,3-*b*]indolizine-3-carboxylate (2g). According to the general procedure **(condition A)**, 1-(pyridin-2-yl)indolizin-2(3*H*)-one (250 mg, 1.19 mmol), Cs_2CO_3 (387 mg, 1.19 mmol) and diethyl 2-(ethoxymethylene) malonate (0.240 mL, 1.19 mmol) were reacted affording **2g** (177 mg, 44%) as yellow/orange crystals. R_f = 0.37 (SiO_2, AcOEt/hexane, 2 : 1); m.p. 252.6 °C. ^{1}H NMR (500 MHz, $CDCl_3$) δ 9.02 (d, J = 9.1 Hz, 1H), 8.83 (s, 1H), 8.67–8.64 (m, 1H), 8.33 (d, J = 6.8 Hz, 1H), 8.23 (d, J = 8.1 Hz, 1H), 7.78 (td, J = 7.8, 1.9 Hz, 1H), 7.41 (ddd, J = 9.1, 6.9, 1.2 Hz, 1H), 7.16 (ddd, J = 7.5, 4.8, 1.1 Hz, 1H), 7.03 (td, J = 6.9, 1.3 Hz, 1H), 4.42 (q, J = 7.1 Hz, 2H), 1.43 (t, J = 7.1 Hz, 3H). ^{13}C NMR (126 MHz, $CDCl_3$) δ 164.8, 158.4, 151.4, 150.4, 148.9, 139.5, 136.7, 133.4, 127.9, 124.3, 122.6, 122.1, 120.9, 114.3, 111.1, 101.7, 101.2, 61.3, 14.5. HRMS (ESI): m/z calcd for $C_{19}H_{15}N_2O_4$, 335.1032 $[M + H]^+$; found, 335.1031.

Diethyl 2-oxo-2*H*-pyrano[2,3-*b*]indolizine-3,10-dicarboxylate (2h). According to the general procedure **(condition A)**, ethyl 2-oxo-2,3-dihydroindolizine-1-carboxylate generated *in situ* (404 mg, 2.00 mmol), Cs_2CO_3 (652 mg, 2.00 mmol) and diethyl 2 (ethoxymethylene)malonate (0.404 mL, 2.00 mmol) were reacted affording **2h** (35 mg, 5%) as yellow crystals. R_f = 0.43 (SiO_2, AcOEt/hexane, 3 : 1); m.p. 227.9 °C. ^{1}H NMR (500 MHz, $CDCl_3$) δ 8.82 (s, 1H), 8.43 (d, J = 8.8 Hz, 1H), 8.37 (d, J = 6.8 Hz, 1H), 7.50 (t, J = 8.8 Hz, 1H), 7.13 (t, J = 6.8 Hz, 1H), 4.42 (q, J = 24.5 Hz, 2H), 4.40 (q, J = 24.5 Hz, 2H), 1.43 (t, J = 21.3, Hz, 3H), 1.40 (t, J = 21.3, Hz, 3H). ^{13}C NMR (126 MHz, $CDCl_3$) δ 164.5, 162.4, 157.6, 152.3, 140.8, 134.0, 129.1, 124.6, 120.4, 115.1, 110.8, 104.2, 93.8, 61.5, 60.5, 14.5, 14.4 ppm. HRMS (ESI): m/z calcd for $C_{17}H_{15}NO_6Na$, 352.0797 $[M + Na]^+$; found, 352.0798.

General procedure for the synthesis of 2-oxo-2*H*-pyrano[2,3-*b*]indolizine-3-carboxylates (condition B)

In a 20 mL Schlenk flask, pyridinium salt (6 mmol, 1 equiv.), potassium carbonate (6 mmol, 1 equiv.) and diethyl 2-(ethoxymethylene)malonate (6 mmol, 1 equiv.) were added and dissolved in 10 mL of DMF. The reaction mixture changed color and was stirred for 24 hours at room temperature. After completion, the mixture was extracted with DCM, and the combined organic layers were dried over Na_2SO_4 and concentrated under reduced pressure. The crude product was purified by column chromatography (silica, AcOEt/hexane 1 : 1).

Diethyl 2-((3-(ethoxycarbonyl)-6-methyl-2-oxo-2*H*-pyrano[2,3-*b*]indolizin-10-yl)methylene)malonate (2i). According to the general procedure **(condition B)**, 1-(2-ethoxy-2-oxoethyl)-2,6-dimethylpyridin-1-ium bromide (450 mg, 2.3 mmol), potassium carbonate (320 mg, 2.3 mmol) and diethyl 2-(ethoxymethylene) malonate (0.467 mL, 2.3 mmol) were reacted affording **2i** (100 mg, 15%) as yellow/orange crystals. R_f = 0.45 (SiO_2, AcOEt/hexane, 3 : 1); m.p. 210.5 °C. ^{1}H NMR (600 MHz, $CDCl_3$) δ 8.92 (s, 1H), 7.77 (s, 1H), 7.65 (d, J = 8.6 Hz, 1H), 7.36 (dd, J = 8.9, 7.1 Hz, 1H), 6.85 (d, J = 7.1 Hz, 1H), 4.53 (q, J = 7.1 Hz, 2H), 4.35 (q, J = 7.1 Hz, 2H), 4.25 (q, J = 7.2 Hz, 2H), 2.86 (s, 3H), 1.34 (t, J = 7.2 Hz, 3H), 1.32 (t, J = 7.2 Hz, 3H), 1.28 (t, J = 7.2 Hz, 3H). ^{13}C NMR (126 MHz, $CDCl_3$) δ 166.7, 165.1, 165.1, 156.5, 151.5, 141.6, 138.9, 138.1, 128.9, 128.7, 124.7, 116.4, 115.1, 113.3, 102.9, 96.9, 62.4, 61.6, 61.5, 22.1, 14.4, 14.2, 14.0 ppm. HRMS (APCI): m/z calcd for $C_{23}H_{22}NO_8$, 442.1345 $[M - H]^-$; found, 440.1350.

General procedure for direct arylation

A Schlenk flask flushed with argon, was charged with ethyl 6-methyl-2-oxo-2*H*-pyrano[2,3-*b*]indolizine-3-carboxylate (0.55 mmol, 1 equiv.), aryl bromide (0.66 mmol, 1.2 equiv.), potassium acetate (1.11 mmol, 2 equiv.), NMP (3 mL) and $PdCl_2(PPh_3)_2$ (0.027 mmol, 0.05 equiv.). The solution was

stirred at 100 °C for 10 min. Afterwards, water (1.11 mmol, 2 equiv.) was added, and the heating was continued at the same temperature overnight. Then, the mixture was cooled to room temperature and extracted with DCM. The combined organic layers were dried over Na_2SO_4 and concentrated under reduced pressure. The crude product was purified by column chromatography (silica, AcOEt/hexane 1 : 1).

Ethyl 10-(4-cyanophenyl)-6-methyl-2-oxo-2*H*-pyrano[2,3-*b*]indolizine-3-carboxylate (3aa). According to the general procedure for direct arylation, ethyl 6-methyl-2-oxo-2*H*-pyrano[2,3-*b*]indolizine-3-carboxylate (0.55 mmol, 1 equiv.), 4-bromobenzonitrile (0.66 mmol, 1.2 equiv.), potassium acetate (1.11 mmol, 2 equiv.), NMP (3 mL), $PdCl_2(PPh_3)_2$ (0.027 mmol, 0.05 equiv.), and water (1.11 mmol, 2 equiv.) were made to react affording **3aa** (120 mg, 60%) as greenish yellow crystals. R_f = 0.45 (SiO_2, AcOEt/hexane, 3 : 1); m.p. 306.1 °C. ^{1}H NMR (600 MHz, $CDCl_3$) δ 9.06 (s, 1H), 7.84–7.81 (m, 2H), 7.80–7.77 (m, 3H), 7.38 (dd, J = 8.9, 7.0 Hz, 1H), 6.89 (d, J = 7.0 Hz, 1H), 4.42 (q, J = 7.1 Hz, 2H), 2.96 (s, 3H), 1.42 (t, J = 7.1 Hz, 3H). ^{13}C NMR (151 MHz, $CDCl_3$) δ 165.3, 157.4, 150.5, 139.4, 138.9, 138.3, 135.1, 132.7, 129.0, 128.0, 118.9, 115.6, 115.4, 112.5, 110.4, 102.3, 101.4, 61.5, 22.3, 14.4 ppm. HRMS (APCI): m/z calcd for $C_{22}H_{15}N_2O_4$, 371.1032 $[M - H]^-$; found, 371.1036.

Ethyl 6-methyl-10-(4-nitrophenyl)-2-oxo-2*H*-pyrano[2,3-*b*]indolizine-3-carboxylate (3ab). According to the general procedure for direct arylation, ethyl 6-methyl-2-oxo-2*H*-pyrano[2,3-*b*]indolizine-3-carboxylate (0.55 mmol, 1 equiv.), 1-bromo-4-nitrobenzene (0.66 mmol, 1.2 equiv.), potassium acetate (1.11 mmol, 2 equiv.), NMP (3 mL), $PdCl_2(PPh_3)_2$ (0.027 mmol, 0.05 equiv.), and water (1.11 mmol, 2 equiv.) were made to react affording **3ab** (25 mg, 50%) as orange crystals. R_f = 0.45 (SiO_2, AcOEt/hexane, 3 : 1); m.p. 284.3 °C. ^{1}H NMR (500 MHz, $CDCl_3$) δ 9.07 (s, 1H), 8.36 (d, J = 8.8 Hz, 2H), 7.89 (d, J = 8.8 Hz, 2H), 7.83 (d, J = 8.9 Hz, 1H), 7.40 (dd, J = 9.0, 7.0 Hz, 1H), 6.91 (d, J = 7.1 Hz, 1H), 4.43 (q, J = 7.1 Hz, 2H), 2.97 (s, 3H), 1.42 (t, J = 7.1 Hz, 3H). ^{13}C NMR (126 MHz, $CDCl_3$) δ 165.3, 157.3, 150.7, 146.3, 139.4, 139.0, 138.3, 137.2, 129.0, 128.2, 124.3, 115.8, 115.5, 112.5, 102.5, 101.1, 61.5, 22.3, 14.4 ppm. HRMS (APCI): m/z calcd for $C_{21}H_{15}N_2O_6$, 391.0930 $[M - H]^-$; found, 391.0932.

Ethyl 10-(4-(*tert*-butyl)phenyl)-6-methyl-2-oxo-2*H*-pyrano[2,3-*b*]indolizine-3-carboxylate (3ac). According to the general procedure for direct arylation, ethyl 6-methyl-2-oxo-2*H*-pyrano[2,3-*b*]indolizine-3-carboxylate (0.20 mmol, 1 equiv.), 1-bromo-4-(*tert*-butyl)benzene (0.26 mmol, 1.2 equiv.), potassium acetate (0.40 mmol, 2 equiv.), NMP (3 mL), $PdCl_2(PPh_3)_2$ (0.010 mmol, 0.05 equiv.), and water (0.40 mmol, 2 equiv.) were made to react affording **3ac** (14 mg, 17%) as orange/brown crystals. R_f = 0.56 (SiO_2, AcOEt/hexane, 2 : 1); m.p. 241.6 °C. ^{1}H NMR (600 MHz, CD_2Cl_2) δ 8.93 (s, 1H), 7.71 (d, J = 8.7 Hz, 1H), 7.57–7.51 (m, 2H), 7.51–7.46 (m, 2H), 7.24 (dd, J = 8.9, 6.9 Hz, 1H), 6.76 (d, J = 7.0 Hz, 1H), 4.27 (q, J = 7.1 Hz, 2H), 2.84 (s, 3H), 1.32–1.29 (m, 12H). ^{13}C NMR (126 MHz, $CDCl_3$) δ 165.7, 158.1, 150.3, 140.1, 138.5, 137.9, 128.9, 128.5, 127.0, 126.8, 125.9, 116.1, 114.9, 112.5, 103.3, 101.1, 61.2, 34.7, 31.3, 22.2, 14.5 ppm. HRMS (APCI): m/z calcd for $C_{25}H_{26}NO_4$, 404.1862 $[M + H]^+$; found, 404.1861.

Procedure for the synthesis of styryl dye

Ethyl 10-formyl-6-methyl-2-oxo-2*H*-pyrano[2,3-*b*]indolizine-3-carboxylate (4a). In a round bottom flask, $POCl_3$ (0.280 mL, 3 mmol) was added to dry DMF (0.310 mL, 4 mmol), at 0 °C. The ice bath was removed and the solution was stirred for 30 min. A solution of ethyl 6-methyl-2-oxo-2*H*-pyrano[2,3-*b*]indolizine-3-carboxylate (0.250 g, 0.92 mmol) in dry DCE (5 mL) was added and the mixture was stirred at 85 °C for 16 hours. After cooling to room temperature, an aqueous solution of saturated sodium acetate (3 mL) was added and heated again for 1 hour at 100 °C, then the reaction mixture was cooled to room temperature and the water-organic layer was extracted with DCM. The combined organic layers were dried over Na_2SO_4 and concentrated under reduced pressure. The crude product was purified by column chromatography (silica, AcOEt/hexane 1 : 1) affording **4a** (230 mg, 83%) as yellow crystals. R_f = 0.40 (SiO_2, AcOEt/hexane, 3 : 1); m.p. 241.4 °C. ^{1}H NMR (500 MHz, $CDCl_3$) δ 10.29 (s, 1H), 9.03 (s, 1H), 8.54 (d, J = 8.8 Hz, 1H), 7.60 (dd, J = 8.8, 7.2 Hz, 1H), 7.05 (d, J = 7.2 Hz, 1H), 4.43 (q, J = 7.1 Hz, 2H), 2.99 (s, 3H), 1.43 (t, J = 7.1 Hz, 3H). ^{13}C NMR (126 MHz, $CDCl_3$) δ 181.8, 164.8, 156.6, 155.8, 140.6, 139.1, 139.0, 131.5, 118.5, 118.0, 112.2, 103.7, 102.3, 61.7, 22.1, 14.4. ppm. HRMS (APCI): m/z calcd for $C_{16}H_{12}NO_5$, 298.0714 $[M - H]^-$; found, 298.0715.

4-Methylpyridinium iodide (5). Synthesis was conducted according to literature.[64] ^{1}H NMR (500 MHz, DMSO-d_6) δ 8.81 (d, J = 6.4 Hz, 2H), 7.94 (d, J = 6.2 Hz, 2H), 4.26 (s, 3H), 2.58 (s, 3H).

(*E*)-4-(2-(3-(Methoxycarbonyl)-6-methyl-2-oxo-2*H*-pyrano[2,3-*b*]indolizin-10-yl)vinyl)-1-methylpyridin-1-ium iodide (6a). In a round bottom flask, 4-methylpyridinium iodide (18 mg, 0.17 mmol), ethyl 10-formyl-6-methyl-2-oxo-2*H*-pyrano[2,3-*b*]indolizine-3-carboxylate (51 mg, 0.17 mmol) and piperidine (0.017 mL) were dissolved in MeOH (4 mL) and refluxed overnight. After cooling down to room temperature, a precipitate is formed, filtered and washed with MeOH to afford ethyl 10-formyl-6-methyl-2-oxo-2*H*-pyrano[2,3-*b*]indolizine-3-carboxylate as red crystals **6a** (25 mg, 37%). M.p. 250.7 °C. ^{1}H NMR (500 MHz, DMSO-d_6) δ 8.94 (s, 1H), 8.78 (d, J = 6.3 Hz, 2H), 8.34–8.19 (m, 4H), 7.68 (t, J = 7.9 Hz, 1H), 7.31 (d, J = 16.0 Hz, 1H), 7.20 (d, J = 7.1 Hz, 1H), 4.23 (s, 3H), 3.81 (s, 3H), 2.95 (s, 3H). ^{13}C NMR (126 MHz, DMSO-d_6) δ 164.9, 156.7, 153.4, 151.7, 145.0, 141.4, 141.2, 139.5, 130.5, 129.0, 123.0, 121.2, 117.4, 115.6, 113.8, 101.1, 99.2, 52.5, 47.0, 21.5 ppm. HRMS (ESI): m/z calcd for $C_{22}H_{19}N_2O_4$, 375.1345.1501 $[M^+]$; found, 375.1348.

Photophysical measurements

HPLC grade solvents were purchased from Sigma-Aldrich and used as obtained. For optical studies, solutions of molecules at low concentrations were used to avoid dimerization or reabsorption effects. All absorption and fluorescence spectra were taken at room temperature (21 °C). A Shimadzu UV/VIS-NIR

spectrophotometer, model UV-3600i Plus, was used for absorption spectra measurement. Fluorescence spectra were recorded with an FS5 spectrofluorometer from Edinburgh Instruments. Fluorescence quantum yields (Φ_{fl}) of molecules in solvents at 21 °C were determined using Coumarin 153 in EtOH (Φ_{fl} = 0.38) and Rhodamine 6 g in EtOH (Φ_{fl} = 0.95) as references. Solutions of low absorbance (A < 0.1) were used to avoid reabsorption or concentration quenching. Refractive index correction for solvents have been performed in the calculations of quantum yields. Molar absorption coefficient, ε, was calculated from the absorbance, A, of a solution of the given molar concentration, c, in a cuvette of length, l, according to Lambert Beer formula:

$$A = c\,\varepsilon\,l$$

Fluorescence kinetics studies were performed using the time correlated single photon counting technique. A modelocked Coherent Mira-HP picosecond laser pumped by a Verdi 18 laser was used for excitation. The fundamental pulses of the Mira laser were up-converted to 387.5 nm. The temporal width of the excitation pulses was ~280 fs and the instrument response function (IRF) about 40 ps. Fluorescence was dispersed with a 0.25 m Jarrell-Ash monochromator and detected with a HMP-100-07 hybrid detector coupled to an SPC-150 PC module, (Becker&Hickl GmbH). Fluorescence decays were analyzed with deconvolution software using a nonlinear least squares procedure with the Marquardt algorithm. A standard χ^2 test and Durbin–Watson (DW) parameter along with residual and autocorrelation function plots were used to assess the quality of a fit. The estimated accuracy for the determination of decay time was below 10 ps.

Computational details

The calculations were performed using the Gaussian 16 program.[65] The solvent effect was introduced in PCM procedure. The SOC elements were also calculated using the Orca program.[66]

Biological studies

The rat embryonic cardiomyoblast-derived H9c2 cells were loaded with the fluorophore at the final concentration of 500 nM in DMEM medium supplemented with 10% foetal bovine serum, 2 mM glutamine, 100 U ml^{-1} penicillin, and 100 μg ml^{-1} streptomycin, and incubated at 37 °C in a humidified atmosphere containing 5% CO_2 for 15 to 60 minutes. After that, the incubation medium was replaced with FluoroBrite™ DMEM. The measurements were performed with the use of an Olympus IX83 confocal microscope with the silicone objective 60× UPLSAPO 60XS. Registered data were transferred to the ImageJ and analysed for presentation.

Author contributions

Conceptualization: D. T. G. and J. S. A. B.; investigation: J. S. A. B., A. W., I. D.; supervision: D. T. G., A. S.; visualization: J. S. A. B., A. W., I. D.; writing – original draft: J. S. A. B., A. W., I. D.; writing – review and editing: D. T. G., J. S. A. B.

All the authors discussed the results and commented on the manuscript.

Data availability

The data supporting this article have been included as part of the ESI.†

Conflicts of interest

There are no conflicts to declare.

Acknowledgements

This work was supported by the Polish National Science Center, Poland (grants OPUS 2020/37/B/ST4/00017 and HARMONIA 2018/30/M/ST5/00460). This project has received funding from the European Union's Horizon 2020 research and innovation programme under the Marie Skłodowka-Curie grant agreement no 101007804. The work was financially supported by the Foundation for Polish Science (TEAM POIR.04.04.00-00-3CF4/16-00). Calculations were performed at the Interdisciplinary Center for Mathematical and Computational Modeling (ICM) University of Warsaw under computational allocation G95-1734. We thank Joseph Milton for amending the manuscript.

References

1 K. Sun, S. Jin, S. Fang, R. Ma, X. Zhang, M. Gao, W. Zhang, T. Lu and D. Du, N-Heterocyclic carbene-catalyzed formal [3 + 3] annulation of alkynoic acid esters with indolin-3-ones: access to functionalized pyrano[3,2-b]indol-2-ones, *Org. Chem. Front.*, 2019, **6**, 2291–2295.

2 X.-Y. Meng, M.-Y. Sun, F.-J. Zhao, Y.-J. Dang, B. Jiang and S.-J. Tu, Domino Reaction of 2,2-Dihydroxyindene-1,3-dione with Aromatic Amines: Efficient Synthesis of Isochromeno[4,3-b]indol-5(11H)-one Derivatives, *Synthesis*, 2014, 3207–3212.

3 N. S. Masterova, S. Yu. Ryabova, L. M. Alekseeva, M. I. Evstratova, S. S. Kiselev and V. G. Granik, Novel pyrano[3,2-b]indole derivatives: synthesis and some properties, *Russ. Chem. Bull.*, 2010, **59**, 637–641.

4 N. Monakhova, J. Korduláková, A. Vocat, A. Egorova, A. Lepioshkin, E. G. Salina, J. Nosek, E. Repková, J. Zemanová, H. Jurdáková, R. Górová, J. Roh, G. Degiacomi, J. C. Sammartino, M. R. Pasca, S. T. Cole, K. Mikušová and V. Makarov, Design and Synthesis of Pyrano[3,2-b]indolones Showing Antimycobacterial Activity, *ACS Infect. Dis.*, 2021, **7**, 88–100.

5 A. P. Gaywood and H. McNab, Methylene Meldrum's Acid Derivatives of Indoxyl and Their Cyclization Reactions under Flash Vacuum Pyrolysis Conditions, *Synthesis*, 2010, 1361–1364.
6 P. C. Unangst and R. E. Brown, Indole esters as heterocyclic synthons. II. Preparation of 1,3-oxazino[5,6-b]indoles and 3-substituted-pyrano[3,2-b]indoles, *J. Heterocycl. Chem.*, 1984, **21**, 283–288.
7 H. K. Kadam and S. G. Tilve, Unique synthesis of isochromenoindolone via reductive-oxidative cyclisation approach, *Indian J. Chem., Sect. B: Org. Chem. Incl. Med. Chem.*, 2019, **58**, 104–108.
8 X. Zhang, W. Hou, D. Zhang-Negrerie, K. Zhao and Y. Du, Hypervalent Iodine-Mediated Intramolecular trans-Aminocarboxylation and Oxoaminocarboxylation of Alkynes: Divergent Cascade Annulations of Isocoumarins under Metal-Free Conditions, *Org. Lett.*, 2015, **17**, 5252–5255.
9 S. Pathak, D. Das, A. Kundu, S. Maity, N. Guchhait and A. Pramanik, Synthesis of 4-hydroxyindole fused isocoumarin derivatives and their fluorescence "Turn-off" sensing of Cu(II) and Fe(III) ions, *RSC Adv.*, 2015, **5**, 17308–17318.
10 J. L. Bullington and J. H. Dodd, Synthesis of tetrahydroindeno[1,2-b]indol-10-ones and their rearrangement to [2]benzopyrano[4,3-b]indol-5-ones, *J. Org. Chem.*, 1993, **58**, 4833–4836.
11 A. Sugimoto, K. Sakamoto, Y. Fujino, Y. Takashima and M. Ishikawa, Synthesis and Inhibitory Effect on Platelet Aggregation of 2-Phenyl-1 (2H)-phthalazinone Derivatives, *Chem. Pharm. Bull.*, 1985, **33**, 2809–2820.
12 A. J. Frew, G. R. Proctor and J. V. Silverton, Reactions of the sodium salts of some heterocyclic β-ketoesters with dimethyl acetylenedicarboxylate, *J. Chem. Soc., Perkin Trans. 1*, 1980, 1251–1256.
13 A. Arcadi, S. Cacchi, F. Marinelli and P. Pace, 5-Alkyl-5-[2-(o-iodophenylcarbamoyl)vinyl] Derivatives of Meldrum's Acid as Substrates for the Intramolecular Heck Reaction: Application to the Synthesis of Carbazoles, *Synlett*, 1993, 743–744.
14 N. L. Nam and I. I. Grandberg, Condensation of oxindole with acetoacetic ester and acetylacetone, *Chem. Heterocycl. Compd.*, 2006, **42**, 1010–1011.
15 W.-Z. Zhang, M.-W. Yang and X.-B. Lu, Carboxylative cyclization of substituted propenyl ketones using CO2: transition-metal-free synthesis of α-pyrones, *Green Chem.*, 2016, **18**, 4181–4184.
16 G. H. Ko, C. Maeng, H. Jeong, S. H. Han, G. U. Han, K. Lee, H. C. Noh and P. H. Lee, Rhodium(III)-Catalyzed Sequential C–H Activation and Cyclization from N-Methoxyarylamides and 3-Diazooxindoles for the Synthesis of Isochromenoindolones, *Chem. – Asian J.*, 2021, **16**, 3179–3187.
17 S. Park, J. Lee, K. J. Shin, E. Oh and J. H. Seo, Consecutive One-Pot versus Domino Multicomponent Approaches to 3-(Diarylmethylene)oxindoles, *Molecules*, 2017, **22**, 503.
18 Q. Chen, Y. Teng and F. Xu, Lanthanide Silylamide-Catalyzed Synthesis of Pyrano[2,3-b]indol-2-ones, *Org. Lett.*, 2021, **23**, 4785–4790.
19 A. S. Kumar and R. Nagarajan, Cyclization Routes for the Synthesis of Functionalized Pyrano[2,3-b]indolones, Pyrazolo[3,4-b]indoles, and Furo[2,3-b]indoles, *Synthesis*, 2013, 1235–1246.
20 M. Abdel-Megid, A versatile molecule for the synthesis of some new polynuclear bioactive heterocyclic systems, *Int. J. Chem.*, 2006, **16**, 149–157.
21 R. Frutos-Pedreño and J.-A. García-López, 2-Arylacetamides as Versatile Precursors for 3-Aminoisocoumarin and Homophthalimide Derivatives: Palladium-Catalyzed Cascade Double Carbonylation Reactions, *Adv. Synth. Catal.*, 2016, **358**, 2692–2700.
22 X. Peng, Y. Huang, W. Wang, S. Li, G. Hao, S. Ren and Y. R. Chi, N-Heterocyclic Carbene-Catalyzed Remote Enantioselective C–C Bond Formation via 1,6-Addition with Formyl Enynes, *ACS Catal.*, 2024, **14**, 2127–2133.
23 A. Kakehi, S. Ito, K. Nakanishi, K. Watanabe and M. Kitagawa, Preparation of New Nitrogen-bridged Heterocycles. A Facile Synthetic Method of Pyrano[2,3-b]indolizinone Derivatives, *Bull. Chem. Soc. Jpn.*, 1980, **53**, 1115–1120.
24 A. Kakehi, S. Ito, K. Watanabe, M. Kitagawa, S. Takeuchi and T. Hashimoto, Preparation of new nitrogen-bridged heterocycles. Synthesis and some reactions of 2,3-dihydroindolizin-2-one derivatives, *J. Org. Chem.*, 1980, **45**, 5100–5104.
25 A. Kakehi, S. Ito, S. Murakami and H. Sano, Preparation of New Nitrogen-bridged Heterocydes. 8. Syntheses of Some Fused Indolizine Derivatives via the Acid-catalyzed Cyclizations of Functionalized 1- and 3-Vinylindolizines, *Bull. Chem. Soc. Jpn.*, 1984, **57**, 548–552.
26 A. Kakehi, S. Ito and K. Matsubara, Preparation of New Nitrogen-Bridged Heterocycles. 39. One-Pot Synthesis of 2H-Pyrano[3,2-a]indolizin-2-one Derivatives, *Bull. Chem. Soc. Jpn.*, 1995, **68**, 2409–2415.
27 G. Jones, W. R. Jackson and A. M. Halpern, Medium effects on fluorescence quantum yields and lifetimes for coumarin laser dyes, *Chem. Phys. Lett.*, 1980, **72**, 391–395.
28 J. A. Van Gompel and G. B. Schuster, Photophysical behavior of ester-substituted aminocoumarins: a new twist, *J. Phys. Chem.*, 1989, **93**, 1292–1295.
29 B. B. Raju and S. M. B. Costa, Photophysical properties of 7-diethylaminocoumarin dyes in dioxane–water mixtures: hydrogen bonding, dielectric enrichment and polarity effects, *Phys. Chem. Chem. Phys.*, 1999, **1**, 3539–3547.
30 M. Sulpizi, P. Carloni, J. Hutter and U. Rothlisberger, A hybrid TDDFT/MM investigation of the optical properties of aminocoumarins in water and acetonitrile solution, *Phys. Chem. Chem. Phys.*, 2003, **5**, 4798–4805.
31 K. Azuma, S. Suzuki, S. Uchiyama, T. Kajiro, T. Santa and K. Imai, A study of the relationship between the chemical structures and the fluorescence quantum yields of coumarins, quinoxalinones and benzoxazinones for the devel-

opment of sensitive fluorescent derivatization reagents, *Photochem. Photobiol. Sci.*, 2003, **2**, 443–449.
32 M. El-Kemary and W. Rettig, Multiple emission in coumarins with heterocyclic substituents, *Phys. Chem. Chem. Phys.*, 2003, **5**, 5221–5228.
33 X. Liu, Z. Xu and J. M. Cole, Molecular Design of UV–vis Absorption and Emission Properties in Organic Fluorophores: Toward Larger Bathochromic Shifts, Enhanced Molar Extinction Coefficients, and Greater Stokes Shifts, *J. Phys. Chem. C*, 2013, **117**, 16584–16595.
34 M. Cavazzini, S. Quici, S. Orlandi, C. Sissa, F. Terenziani and A. Painelli, Intimately bound coumarin and bis(alkylaminostyryl)benzene fragments: synthesis and energy transfer, *Tetrahedron*, 2013, **69**, 2827–2833.
35 D. Kim, S. Singha, T. Wang, E. Seo, J. H. Lee, S.-J. Lee, K. H. Kim and K. H. Ahn, In vivo two-photon fluorescent imaging of fluoride with a desilylation-based reactive probe, *Chem. Commun.*, 2012, **48**, 10243–10245.
36 I. Kim, D. Kim, S. Sambasivan and K. H. Ahn, Synthesis of π-Extended Coumarins and Evaluation of Their Precursors as Reactive Fluorescent Probes for Mercury Ions, *Asian J. Org. Chem.*, 2012, **1**, 60–64.
37 D. Kim, Q. P. Xuan, H. Moon, Y. W. Jun and K. H. Ahn, Synthesis of Benzocoumarins and Characterization of Their Photophysical Properties, *Asian J. Org. Chem.*, 2014, **3**, 1089–1096.
38 Y. W. Jun, H. R. Kim, Y. J. Reo, M. Dai and K. H. Ahn, Addressing the autofluorescence issue in deep tissue imaging by two-photon microscopy: the significance of far-red emitting dyes, *Chem. Sci.*, 2017, **8**, 7696–7704.
39 Y. J. Reo, Y. W. Jun, S. W. Cho, J. Jeon, H. Roh, S. Singha, M. Dai, S. Sarkar, H. R. Kim, S. Kim, Y. Jin, Y. L. Jung, Y. J. Yang, C. Ban, J. Joo and K. H. Ahn, A systematic study on the discrepancy of fluorescence properties between in solutions and in cells: super-bright, environment-insensitive benzocoumarin dyes, *Chem. Commun.*, 2020, **56**, 10556–10559.
40 Y. Jung, N. K. Park, S. Kang, Y. Huh, J. Jung, J. K. Hur and D. Kim, Latent turn-on fluorescent probe for the detection of toxic malononitrile in water and its practical applications, *Anal. Chim. Acta*, 2020, **1095**, 154–161.
41 A. Mukhopadhyay, T. Hossen, I. Ghosh, A. L. Koner, W. M. Nau, K. Sahu and J. N. Moorthy, Helicity-Dependent Regiodifferentiation in the Excited-State Quenching and Chiroptical Properties of Inward/Outward Helical Coumarins, *Chem. – Eur. J.*, 2017, **23**, 14797–14805.
42 A. Mukhopadhyay, V. K. Maka and J. N. Moorthy, Remarkable influence of 'phane effect' on the excited-state properties of cofacially oriented coumarins, *Phys. Chem. Chem. Phys.*, 2017, **19**, 4758–4767.
43 A. Kakehi, S. Ito, H. Suga, S. Takano and K. Hirata, Preparation of New Nitrogen-Bridged Heterocycles. 45. Smooth Hydrolysis of 6-Membered Heterocyclic 2-Imines with Partial Aromaticity, *Chem. Pharm. Bull.*, 1998, **46**, 1632–1634.
44 C. Galli, "CESIUM ION EFFECT" AND MACROCYCLIZATION. A CRITICAL REVIEW, *Org. Prep. Proced. Int.*, 1992, **24**, 285–307.
45 S. S. Bhalodiya, M. P. Parmar, D. B. Upadhyay, C. D. Patel, D. P. Vala, D. Rajani and H. M. Patel, Cs2CO3-promoted one-pot synthesis of novel tetrahydrobenzofuran-4(2*H*)-ones: *In vitro* antimicrobial, antimalarial activity and *in silico* docking study, *Results Chem.*, 2024, **7**, 101304.
46 P. A. Khardina, E. M. Buev, V. S. Moshkin and V. Y. Sosnovskikh, Novel synthesis of 2,3-dihydrobenzofuran-3-amines from salicylic aldehydes: Trimethylsilyl as traceless activating group, *Tetrahedron Lett.*, 2024, **139**, 154992.
47 P. Li, Y. Ji, W. Chen, X. Zhang and L. Wang, The facile synthesis of 2-bromoindoles via Cs2CO3-promoted intramolecular cyclization of 2-(gem-dibromovinyl)anilines under transition-metal-free conditions, *RSC Adv.*, 2012, **3**, 73–78.
48 J. Ezquerra and J. Alvarez-Builla, 2-Methylpyridinium salts as 1,4-dinucleophiles. II. Westphal condensation with substituted pyridinium substrates, *J. Heterocycl. Chem.*, 1986, **23**, 1151–1157.
49 Z. Chen, S. Zhang, X. Qi, S. Liu, Q. Zhang and Y. Deng, Fluorescent quinolizinium ionic liquids (salts) with unexpectedly high quantum yields up to >99%, *J. Mater. Chem.*, 2011, **21**, 8979–8982.
50 T. S. Chinta Rao, S. Saha, G. B. Raolji, B. Patro, P. Risbood, M. J. Difilippantonio, J. E. Tomaszewski and S. V. Malhotra, Microwave assisted Westphal condensation and its application to synthesis of sempervirine and related compounds, *Tetrahedron Lett.*, 2013, **54**, 487–490.
51 J. V. Greenhill, H. Loghmani-Khouzani and D. J. Maitland, Tautomerism in ketomethylquinolines. Part 2. Further results on 2-ketomethylquinolines, *J. Chem. Soc., Perkin Trans. 1*, 1991, 2831–2840.
52 A. Kakehi, S. Ito and T. Yotsuya, Preparation of New Nitrogen-Bridged Heterocycles. XIII.: Syntheses of Some Tricyclic and Tetracyclic Indolizine Derivatives with Antiallergic Activity, *Chem. Pharm. Bull.*, 1986, **34**, 2435–2442.
53 S. Wu, Q. Cao, X. Wang, K. Cheng and Z. Cheng, Design, synthesis and biological evaluation of mitochondria targeting theranostic agents, *Chem. Commun.*, 2014, **50**, 8919–8922.
54 A. S. Brown, L.-M. Bernal, T. L. Micotto, E. L. Smith and J. N. Wilson, Fluorescent neuroactive probes based on stilbazolium dyes, *Org. Biomol. Chem.*, 2011, **9**, 2142–2148.
55 Y. Liu, B. Wang, J.-T. Hou, P. Xie, W. Li and S. Wang, Molecular engineering and bioimaging applications of C2-alkenyl indole dyes with tunable emission wavelengths covering visible to NIR light, *Bioorg. Chem.*, 2023, **141**, 106905.
56 12 Principles of Green Chemistry, **https://www.acs.org/greenchemistry/principles/12-principles-of-green-chemistry.html**, (accessed 31 July 2024).
57 G. Kobayashi, Y. Matsuda, R. Natsuki, Y. Tominaga, T. Okamura and A. Itamura, Studies on Indole Derivatives. XVII. The Synthesis of Indoxyl Derivatives. (3) The

Reactions of 3-Hydroxy-2-(1-methylthiovinyl)-indole Derivatives with Amines, *Yakugaku Zasshi*, 1973, **93**, 964–970.

58 R. R. Valiev, V. N. Cherepanov, G. V. Baryshnikov and D. Sundholm, First-principles method for calculating the rate constants of internal-conversion and intersystem-crossing transitions, *Phys. Chem. Chem. Phys.*, 2018, **20**, 6121–6133.

59 A. Manian, R. A. Shaw, I. Lyskov, W. Wong and S. P. Russo, Modeling radiative and non-radiative pathways at both the Franck–Condon and Herzberg–Teller approximation level, *J. Chem. Phys.*, 2021, **155**, 054108.

60 A. Kawski, On the Estimation of Excited-State Dipole Moments from Solvatochromic Shifts of Absorption and Fluorescence Spectra, *Z. Naturforsch., A: Phys. Sci.*, 2002, **57**, 255–262.

61 Ł. Kielesiński, I. Deperasińska, O. Morawski, K. V. Vygranenko, E. T. Ouellette and D. T. Gryko, Polarized, V-Shaped, and Conjoined Biscoumarins: From Lack of Dipole Moment Alignment to High Brightness, *J. Org. Chem.*, 2022, **87**, 5961–5975.

62 Z. R. Grabowski, K. Rotkiewicz and W. Rettig, Structural Changes Accompanying Intramolecular Electron Transfer: Focus on Twisted Intramolecular Charge-Transfer States and Structures, *Chem. Rev.*, 2003, **103**, 3899–4032.

63 G. Dyker and O. Muth, Synthesis of Methylene- and Methine-Bridged Oligopyridines, *Eur. J. Org. Chem.*, 2004, 4319–4322.

64 K. Senthil, S. Kalainathan and A. R. Kumar, Effect of additives on the large-size growth of 4-N,N-dimethylamino-4-N-methyl stilbazolium naphthalene-2-sulfonate (DSNS) single crystal: an efficient stilbazolium derivative NLO crystal with potential terahertz wave properties, *CrystEngComm*, 2014, **16**, 9847–9856.

65 M. J. Frisch, G. W. Trucks, H. B. Schlegel, G. E. Scuseria, M. A. Robb, J. R. Cheeseman, G. Scalmani, V. Barone, G. A. Petersson, H. Nakatsuji, X. Li, M. Caricato, A. V. Marenich, J. Bloino, B. G. Janesko, R. Gomperts, B. Mennucci, H. P. Hratchian, J. V. Ortiz, A. F. Izmaylov, J. L. Sonnenberg, D. Williams-Young, F. Ding, F. Lipparini, F. Egidi, J. Goings, B. Peng, A. Petrone, T. Henderson, D. Ranasinghe, V. G. Zakrzewski, J. Gao, N. Rega, G. Zheng, W. Liang, M. Hada, M. Ehara, K. Toyota, R. Fukuda, J. Hasegawa, M. Ishida, T. Nakajima, Y. Honda, O. Kitao, H. Nakai, T. Vreven, K. Throssell, J. A. Montgomery, J. E. Peralta Jr., F. Ogliaro, M. J. Bearpark, J. J. Heyd, E. N. Brothers, K. N. Kudin, V. N. Staroverov, T. A. Keith, R. Kobayashi, J. Normand, K. Raghavachari, A. P. Rendell, J. C. Burant, S. S. Iyengar, J. Tomasi, M. Cossi, J. M. Millam, M. Klene, C. Adamo, R. Cammi, J. W. Ochterski, R. L. Martin, K. Morokuma, O. Farkas, J. B. Foresman and D. J. Fox, *Gaussian 16 (Revision A.03)*, Gaussian Inc., Wallingford CT, 2016.

66 F. Neese, Software update: the ORCA program system, version 4.0, *Wiley Interdiscip. Rev.: Comput. Mol. Sci.*, 2018, **8**, e1327.